Journal of Catalysis **211,** 511–520 (2002)
doi:10.1006/jcat.2002.3766

Selective Half-Hydrogenation of Adiponitrile to Aminocapronitrile on Ni-based Catalysts Elaborated from Lamellar Double Hydroxide Precursors

Didier Tichit,* Robert Durand,* Alice Rolland,* Bernard Coq,*,[1] Joseph Lopez,† and Philippe Marion†

*Laboratoire de Matériaux Catalytiques et Catalyse en Chimie Organique, UMR CNRS-ENSCM 5618, ENSCM, 8 rue d l'Ecole Normale, 34296 Montpellier Cedex 5, France; and †Rhodia, Centre de Recherche de Lyon, 85, avenue des Frères Perret, BP 62, 69192 Saint-Fons Cedex, France

Received May 1, 2002; revised July 5, 2002; accepted July 5, 2002

Layered double hydroxides with a hydrotalcite-like structure and containing $Ni^{2+}/Mg^{2+}/Al^{3+}$ cations in different amounts were prepared and activated under various conditions. These catalysts were tested in the liquid-phase hydrogenation of adiponitrile with the aim of producing aminocapronitrile (ACN). The reaction was carried out in a batch reactor at 323–353 K and 2.5 MPa H_2 pressure with catalysts reduced at 823 K. The products were ACN, hexamethylenediamine (HMDA), azacycloheptane (ACH), and C_{12} compounds. The ACH and C_{12} byproducts are formed by condensation between "imine-" and "amine-like" adsorbed species on metal and acid sites (bifunctional mechanism), and on the metal sites as well. The tuned addition of Mg ($Mg/(Mg + Ni) = 0.20$) allows us to reach the highest selectivity and yield in ACN (66% selectivity at 70% conversion, 50% yield at 85% conversion). The IR spectroscopy of adsorbed CO provided evidence of the presence of smaller Ni^0 ensembles on the sample with $Mg/(Mg + Ni) = 0.20$, as well as larger back-donation from Ni^0 sites to the $2\pi^*$ orbitals of CO. On that account, it is proposed that the lower formation of HMDA, ACH, and C_{12} byproducts may be mainly due to (i) a faster desorption of ACN from the Ni^0 surface before deeper hydrogenation and (ii) the decrease of transimination reactions which need large Ni^0 ensembles to proceed. The correlation between acidity and condensation reactions is not obvious, since upon Mg substitution for Ni, the number of acid sites increases but their strength decreases concurrently, as shown by temperature-programmed desorption of NH_3. © 2002 Elsevier Science (USA)

INTRODUCTION

1-Amino-5-cyanopentane (aminocapronitrile, ACN) is the key intermediate in a new route for synthesis of caprolactam for the fabrication of nylon-6 (1). An elegant catalytic route could be considered through the partial hydrogenation of 1,4-dicyanobutane (adiponitrile, ADN) over heterogeneous catalysts. The challenge is to stop the reaction halfway to avoid deep hydrogenation to 1,6-diaminohexane (hexamethylenediamine, HMDA). A few catalytic materials have been described as selective in this transformation. A first patent which dates back to 1952 claims 92% ACN yield with the use of Pd/silica-gel in a liquid-phase process at 30 MPa, 383 K, and a large excess of NH_3 (2). In a gas-phase process, 100% ACN selectivity at 52% ADN conversion was claimed on K-doped Ni/Fe_2O_3 (3), and $Ni/\alpha\text{-}Al_2O_3$ (4) catalysts with a reactants molar ratio $H_2/ADN \approx 300$. High ACN selectivities have also been obtained in the liquid-phase hydrogenation of ADN by using catalysts containing Rh supported on high-surface MgO, and performing the reaction in the presence of a large excess of NH_3 (5). Yields of ca. 64% were thus claimed in the hydrogenation at 373 K of ADN on 5 wt% Rh/Al_2O_3 in a batch reactor and of 3 MPa H_2 pressure with a large excess of tetrahydrofuran and NH_3 as solvents (6). A 35% Ni/MgO promoted with Fe yielded 71.3% ACN in the hydrogenation of ADN in a batch reactor under 7 MPa H_2 pressure with a large excess of NH_3 or methanol (10/1, vol/vol) with respect to ADN (7). With lower NH_3 excess, a powdered promoted Fe-based catalyst gave 56.8% yield in a continuous process operating at 25 MPa (8). Raney Ni catalysts exhibited good ACN selectivities when the reaction was carried out in excess of NH_3, or methanol with an inorganic base (9). The hydrogenation at 323 K and 2 MPa of concentrated HMDA solution of ADN over a promoted Raney Ni catalyst lead to an ACN yield of ca. 56% at 84% ADN conversion with a small addition of H_2O and KOH (10). Depending on the processes, the main secondary products are HMDA from deep hydrogenation of ACN, azacycloheptane (ACH), and condensed C_{12} amines (BHT); the latter products are formed by inter- and intratransimination between imine and amine intermediates (9, 11, 12). From these selected examples it comes out that a high dilution of ADN, especially by methanol or NH_3, favors the ACN selectivity. However, this is detrimental to productivity. On the other hand, Ni-based materials are excellent candidates for preparing active and selective catalysts.

[1] To whom correspondence should be addressed. E-mail: coq@cit.enscm.fr.

0021-9517/02 $35.00

We have recently shown that lamellar Ni-containing double hydroxides (LDH) are efficient precursors for catalysts that are very selective in the hydrogenation of nitriles (13, 14). In particular, a catalyst obtained from Ni/Mg/Al (0.42/1.43/1) LDH yielded 91.7% ethylamine in the gas-phase hydrogenation of acetonitrile at 393 K and atmospheric pressure (13). There is an optimal Mg content resulting from a compromise between the reducibility of Ni and the acidity of the material, both decreasing with the introduction of Mg. An increase in basicity indeed favors the desorption of amine and decreases to some extent the transimination reactions between amines and imines. In their pioneering work on the liquid-phase hydrogenation of nitriles, von Braun *et al.* (15) claimed that these condensation steps occur in the homogeneous phase, but Dallons *et al.* (16) concluded that the transimination reactions take place at the catalyst surface. On supported metal catalysts two pathways can exist for the formation of byproducts at the catalyst surface:

(1) A condensation reaction between adsorbed imine and amine proceeding at the metal surface (17, 18).

(2) On supported metal catalysts, the condensation between amine and protonated imine can also occur on acidic sites of the carrier to yield a protonated aminal, which in turn loses NH_3 giving a secondary imine, further hydrogenated to amine at metal sites; this is a bifunctional mechanism (13, 19, 20).

Moreover, due to the presence of both Al and Mg, such materials can be easily shaped, and thereby constitute attractive candidates as catalytic materials for the partial hydrogenation of ADN to ACN. It is worth noting that LDH-like materials of widely varying compositions have recently been claimed as active in the deep hydrogenation of dinitriles (21). This is the aim of this study to evaluate Ni-based LDH as precursors for the selective hydrogenation of ADN to ACN in the liquid phase.

EXPERIMENTAL

Preparation and Characterization of the Materials

LDH materials containing $Ni^{2+}/Mg^{2+}/Al^{3+}$ cations with a large range of compositions were prepared. They were obtained by coprecipitation at constant pH of 11 ± 0.2 of an aqueous solution containing in appropriate amounts $Ni(NO_3)_2 \cdot 6H_2O$, $Mg(NO_3)_2 \cdot 6H_2O$, and $Al(NO_3)_3 \cdot 9H_2O$ with a solution of NaOH (1 M). The dropwise addition was performed at 293 K under vigorous stirring. The precipitated gels were heated at 353 K during 15 h, centrifugated, and washed several times with demineralized water until neutral pH was obtained. The solids were finally dried in an oven at 353 K for 20 h. The chemical analyses of the solids were carried out at the Service Central d'Analyse du CNRS (Solaize, France) by ICP-MS. Compositions of the samples are given in Table 1. The ratio ($\Sigma M^{2+}/Al^{3+}$) was fixed at 3 in the starting synthesis solution for samples AR39, AR44, AR5, and AR6, and at 2 for sample AR7. The chemical composition of the solids is generally close to that of the synthesis solution. The presence of carbonates comes from CO_2 in the surrounding atmosphere. We have assigned carbonate species to CO_3^{2-} alone, but part of these species are HCO_3^- (22), which explains the excess of negative charge found in some samples. The remaining Na content from precipitation procedure never exceeded 100 ppm. The samples for catalysis were reduced for 2 h at 823 or 893 K in H_2/N_2 (20/80, vol/vol) flow (150 $cm^3\ min^{-1}$, ramp: 3 K min^{-1}).

The materials were characterized by X-ray diffraction, N_2 sorption at 77 K, temperature-programmed reduction by H_2 (TPR), H_2 chemisorption, IR spectroscopy of adsorbed CO, and temperature-programmed desorption of NH_3.

XRD patterns were recorded on a CGR Theta 60 instrument using monochromatized Cu $K\alpha 1$ radiation at $\lambda = 1.5405$ Å (40 kV and 50 mA). N_2 sorption was performed at 77 K with a Micromeritics ASAP 2000 set-up. Before N_2 sorption, the sample was outgassed at 523 K at 10^{-4} Pa. The surface areas were determined using the BET equation.

TPR by H_2 (H_2/Ar: 3/97, flow = 30 $cm^3\ min^{-1}$, $m = 30$ mg, ramp = 10 K min^{-1}) was carried out with a Micromeritics AutoChem 2910 apparatus using TCD detection. The H_2 consumption was determined after H_2O was trapped at ca. 200 K. TPR experiments were run with the aim to determine the degree of reduction of Ni before chemisorption. The TPR were carried out after *in situ* reactivation of the sample under the same conditions as those for H_2 chemisorption (vide infra).

TABLE 1

Some Characteristics of the Ni/Mg/Al LDHs

Sample	Chemical formula[a]	(Mg + Ni)/Al	Mg/(Mg + Ni)	$\Sigma(2CO_3^{2-} + NO_3^-)/Al^{3+}$
AR39	$[Ni_{0.74}Al_{0.25}(OH)_2](CO_3^{2-})_{0.05}(NO_3^-)_{0.18} \cdot mH_2O$	2.92	0.0	1.02
AR44	$[Ni_{0.67}Mg_{0.07}Al_{0.25}(OH)_2](CO_3^{2-})_{0.04}(NO_3^-)_{0.18} \cdot mH_2O$	2.96	0.095	1.04
AR5	$[Ni_{0.60}Mg_{0.15}Al_{0.25}(OH)_2](CO_3^{2-})_{0.09}(NO_3^-)_{0.18} \cdot mH_2O$	3.00	0.20	1.29
AR7	$[Ni_{0.49}Mg_{0.14}Al_{0.36}(OH)_2](CO_3^{2-})_{0.06}(NO_3^-)_{0.25} \cdot mH_2O$	1.76	0.22	1.03
AR6	$[Ni_{0.45}Mg_{0.29}Al_{0.26}(OH)_2](CO_3^{2-})_{0.09}(NO_3^-)_{0.18} \cdot mH_2O$	2.89	0.39	1.36

[a] After drying at 353 K; trace amounts of Na (<100 ppm) were identified in some samples.

The accessibility to Ni^0 phase was estimated by volumetry of H_2 chemisorption with a Micromeritics ASAP 2010 and a dedicated attachment. The sample was reactivated at 773 K in H_2 for 2 h, then outgassed at the same temperature for 1 h at 10^{-4} Pa. The Ni surface was then saturated by step with H_2 at 373 K until 40–50 kPa was reached. The H_2 uptake was estimated by the extrapolation to zero pressure of the linear part of the isotherm.

In situ DRIFT experiments of adsorbed CO were conducted on a Bruker Equinox 55 spectrometer with a special cell (Graseby Specac) allowing a gas flow and high temperature operation. A sample of 80 mg of powder was reactivated in flowing H_2 overnight at 723 K, then outflowed with Ar at the same temperature for 2 h. After cooling to room temperature in Ar, CO/He (1/99) was fed to the reactor cell. After evacuation of gaseous CO with Ar, the collection of IR spectra (100 scans, resolution 4 cm^{-1}) was started from RT to 523 K by step of 20 to 30 K.

NH_3-TPD experiments were carried out using a Micromeritics Autochem 2910 with TCD detection. NH_3 was adsorbed at 373 K on the reduced and outgassed catalysts. Heating was then started up to 873 K at 10 K min^{-1} in He flow.

Catalytic Experiments

The liquid-phase hydrogenation of ADN was carried out in a tank reactor (100 cm^3) under strirring at 323–353 K and 2.5 MPa H_2 pressure. An aliquot of the passivated catalyst (400–500 mg, grain size: 63–125 μm) was first reactivated in situ in HMDA (24 g) with various amounts of water and KOH. The reactivation was carried out for 2 h at 423 K and 3.5 MPa H_2 pressure. After cooling to the reaction temperature (generally 353 K), the solution was purged with N_2 flow. The reactant ADN ($m = 25$ g) was then pushed into the reactor by H_2 flow. The H_2 pressure was then maintained constant into the reactor at 2.5 MPa by H_2 feed regulation. The consumption of H_2 was monitored by a pressure transducer in an upstream reservoir. The initial reaction rate was determined from H_2 consumption, and samples of reaction mixture were withdrawn from the reactor from 50 to 90% ADN conversion. The sample compositions were analyzed offline by gas chromatography (Varian 3300) on a Restek RTX-2 amine capillary column (30 m; i.d., 0.25 mm).

The concentration of reactant and products in the withdrawn samples was determined with respect to the internal standard diphenylether. Thereafter, the selectivity to the product i has been expressed as the number of moles of ADN which has reacted to i divided by the total number of moles of transformed ADN:

For uncondensed C_6 products (ACN, HMDA, ACH),

$$S_i = 100\frac{\mathrm{mol}_i}{(\mathrm{mol}_0 - \mathrm{mol}_t)_{\mathrm{ADN}}}.$$

For condensed C_{12} products (BHT),

$$S_i = 100\frac{2\mathrm{mol}_i}{(\mathrm{mol}_0 - \mathrm{mol}_t)_{\mathrm{ADN}}}.$$

The sum of product selectivities should be 100%. Actually, in most of the experiments it was lower (92–95%). The imbalance should be accounted for by condensed imines (C_{12} imines), which are quite unstable during the GC analysis. Some parallel measurements of imine concentration by a polarographic method or NMR have shown that the deficit of identified products in the reaction can be accounted for by these heavier imines.

The properties of these materials were compared with those of a commercial Raney-type Ni catalyst (STREM).

RESULTS AND DISCUSSION

Characterization of the Materials

The XRD patterns of precursor materials are those of well-crystallized LDH. No excess phase was identified showing that Ni^{2+} was isomorphously substituted for Mg^{2+} in the layers. The XRD patterns show the appearance of Ni^0 phase upon reduction at 823 K.

The textural properties of the materials strongly depend on the thermal treatments. The uncalcined lamellar structure exhibits low surface area of 15–35 $m^2\ g^{-1}$, which increases upon thermal treatment at high temperature. The S_{BET} values are given in Table 2 for every sample after reduction at 823 K of the materials. The highest surface area was found for AR5 ($Mg/Mg + Ni) = 0.20$, $S_{BET} = 290\ m^2\ g^{-1}$). The surface area of the calcined and/or reduced samples depends on their chemical composition, which determined the relative amounts of mixed oxide and spinel-like phases. The former leads to higher surface area than the latter, which is favored at high Ni content (23). The best compromise between these phases is obtained for

TABLE 2

BET Surface Area, H_2/Ni Molar Consumption Ratio in the Various TPR Experiments, and Accessibility to Ni Sites

Sample	S_{BET}[a] ($m^2\ g^{-1}$)	H_2/Ni[b]	H_2/Ni[c]	H/Ni[d]	Ni^0 accessible sites (mmol g^{-1})
AR39	166	0.94	0.07	0.05	0.52
AR44	176	0.90	—	0.08	0.82
AR5	293	0.99	0.30	0.10	0.95
AR7	220	1.12	0.32	0.065	0.63
AR6	172	0.86	0.38	0.05	0.35

[a] After drying at 393 K and reduction at 823 K.

[b] From TPR experiments of the dried samples at 393 K (H_2 uptake at $T > 580$ K).

[c] From TPR experiments of the reduced samples then in situ reactivated at 773 K in H_2.

[d] After drying at 393 K and reduction at 823 K.

AR5. If the reduction of AR5 is carried out at 893 K, the S_{BET} decreases to 165 m^2 g^{-1}. All the samples exhibit a T4-type histeresis loop for N_2 desorption. The curves provide evidence for the absence of microporosity, and a mean mesopore size of 5–7 nm.

The TPR profiles of the LDH samples are given in Fig. 1A. Two peaks of H_2 consumption are observed with maxima at 550 K for the first and ranging from 700 to 900 K for the second. The maximum of the second broad peak is regularly shifted toward higher temperatures when the Mg content increases. In a detailed previous study on the reduction of Ni-containing LDH (23), we clearly demonstrated with mass spectrometry coupling that the first H_2 consumption peak at 550 K comes from the reduction of nitrate anions mainly to NO. In full agreement with this fact, the H_2 consumption represented by the broad peak at high temperature is very close to that corresponding to the reduction of Ni^{2+} into Ni^0 in the present samples. In these TPR experiments (dynamic conditions, $H_2/Ar = 3/97$), it thus appears that almost full Ni reduction is achieved at 1000 K for the less reducible sample AR6. Since the materials are reduced at 823 K in pure H_2 overnight to yield the catalysts, it is of utmost importance to know the degree of Ni reduction in the catalysts after this treatment. That is why we carried out TPR experiments after reactivation of some reduced catalysts at 823 K in flowing H_2 overnight (Fig. 1B). The remaining H_2 consumption shows that the degree of Ni reduction in the catalyst ranges from 62% in AR6 (high Mg content) to 93% in the Mg-free AR39.

The accessibility to the Ni^0 phase was estimated from H_2 chemisorption. The data are collected in Table 2 for the uncalcined samples directly reduced at 823 K. The accessibility to Ni goes through a maximum value ca. 10% for AR5. It is worth noting the good accessibility to the Ni^0 phase in spite of the very high Ni loading of 68%. In comparison, a H/Ni ratio of ca. 0.18 was reported for a 21%Ni/MgO reduced at 673 K (24).

All these observations are in perfect agreement with the previous detailed study on the activation of Ni- and Mg-containing LDH (23).

Catalytic Experiments

The possible occurrence of interparticle mass transfer limitations was checked on the most active sample: Raney Ni. The rotation speed was varied from 100 to 900 rpm; the initial rate reached a plateau value between 700 and 800 rpm, then decreased after appearance of a vortex. The value of 730 rpm was then chosen for any further experiments. Intraparticle mass transfer was checked with AR5 by sieving two fractions, <63 μm and 63–125 μm; the catalytic data were the same.

In the course of ADN selective hydrogenation over LDH-originating catalysts, the target product is ACN, with

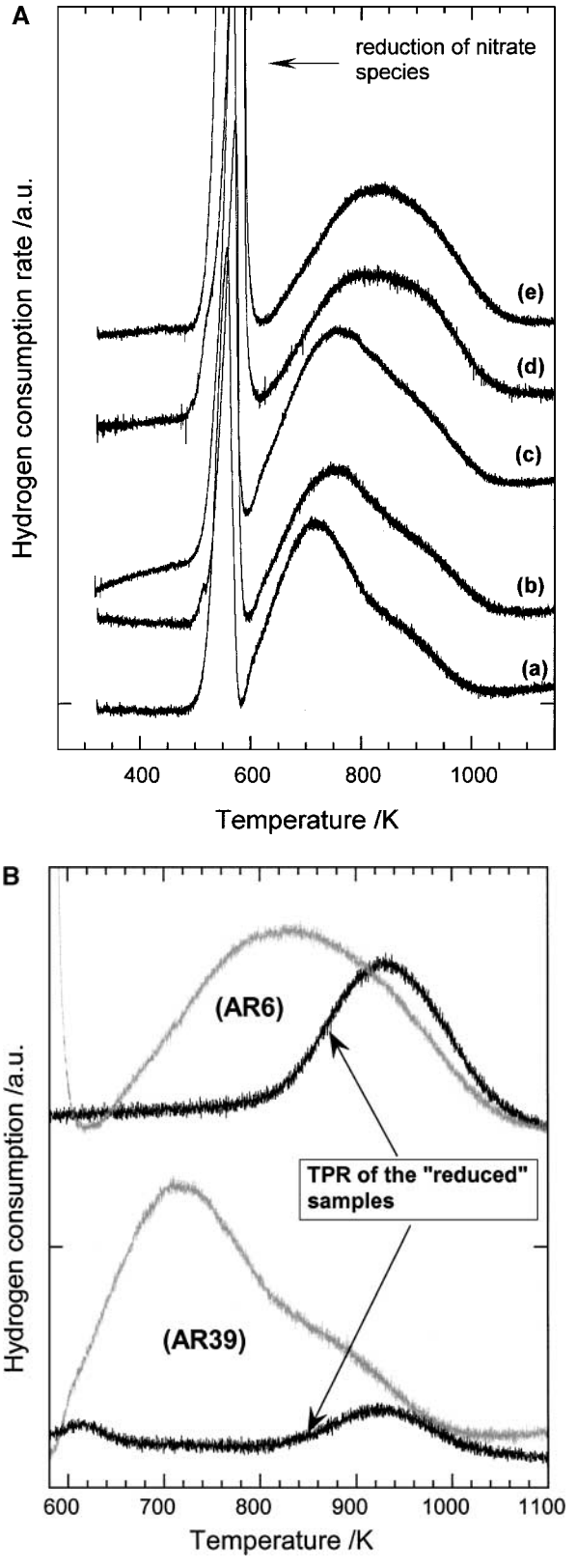

FIG. 1. (A) H_2-TPR profiles of Ni/Mg/Al LDH precursors; (a) AR39, (b) AR44, (c) AR5, (d) AR7, (e) AR6; conditions: H_2/Ar (3/97), ramp: 10 K min^{-1}. (B) H_2-TPR profiles of AR39 and AR6 catalysts after reduction at 823 K; conditions: H_2/Ar (3/97), ramp: 10 K min^{-1}.

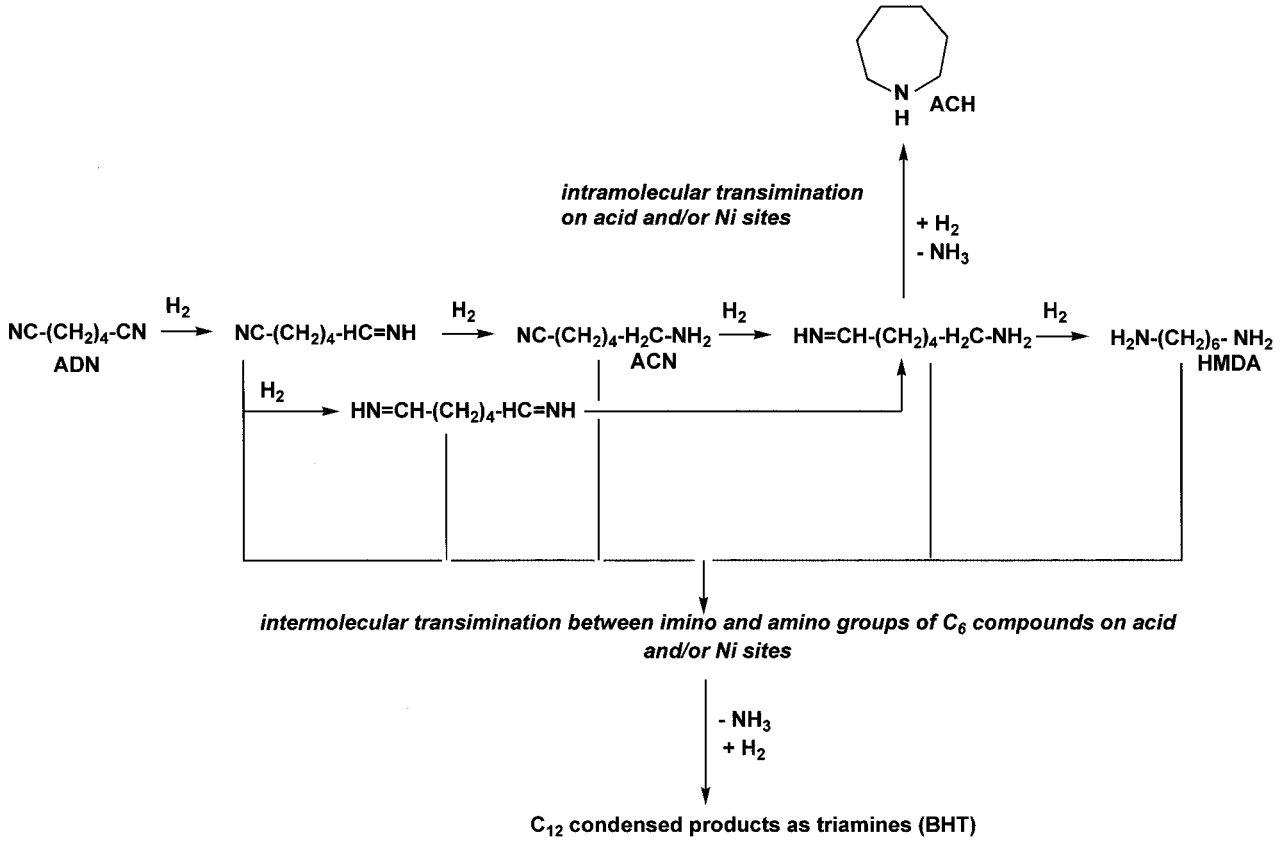

FIG. 2. Formal reaction scheme for adiponitrile hydrogenation.

HMDA, ACH, and C_{12} compounds as byproducts. This is obviously in line with the general scheme of α, ω-dinitrile hydrogenation (5, 9, 11, 12). It is worth noting that in spite of the presence of KOH, the well-known Thorpe–Ziegler intramolecular condensation of ADN to 2-aminomethylcyclopentylamine (C–C bond formation) was not occurring (11, 12). A simplified representation of this scheme with the products only detected in our experiments is displayed in Fig. 2. There are several types of transimination between imino and amino groups. One leads to dimeric compounds when transimination occurs between the imino intermediate compounds and an amine. The second type is the intramolecular transimination of 1-amino-6-imino-hexane intermediate yielding ACH.

Before discussing the main point in this study, which is the influence of catalyst composition on the reaction, we shall first present the effect of operating conditions on the catalytic properties, i.e., the presence of KOH and water, the temperature of in situ reactivation, and the reconstruction of the layered structure of the material by water.

Parametric study. The addition in the reaction medium of a certain amount of an inorganic base is recommended to improve the selectivity to aminonitrile in the hydrogenation of dinitriles on Raney Ni (9, 21). In the case of the present Ni-based catalysts from LDH precursors, the same behavior occurs as shown by the data reported in Table 3. The trace amounts of Na (<100 ppm) found in some samples cannot interfere with the effect of KOH since the ratio Na/K is ca. 1/50 mol/mol. In the absence of KOH, the loss of selectivity occurs by transimination with the formation of ACH mainly. Ziemecki (9) interpreted the promoter effect of inorganic base addition by the stabilization of an intramolecular interaction of ACN to an heterocyclic form containing imino form of the CN group. Such cyclic conformation would impede readsorption of the amino-nitrile, and its further hydrogenation to 1-amino-6-imino-hexane. However, KOH addition should neutralize some acid sites responsible for the intramolecular condensation of 1-amino-6-imino-hexane to ACH. Neutralization of acid sites was indeed postulated to interprete the better selectivity to butylamine in the hydrogenation of butyronitrile over Raney Ni in the presence of NaOH (25). It is obvious that the doping effect of KOH addition is determined by its adsorption isotherm; the latter being likely different depending on H_2O content and the nature of the catalyst. Fundamental studies are further needed to better understand that point. However, it is worth noting that the same KOH addition was found optimum in order to promote the selectivity of Raney Ni in the present work.

TABLE 3

Catalytic Properties of AR5 Catalysts for the Hydrogenation of Adiponitrile at 70% Conversion

	Initial rate (mol g^{-1} s^{-1})	Selectivities (mol%)			
		ACN	HMDA	ACH	BHT
KOH addition in mol/mol_{Ni} (other conditions: 9.6 vol% H_2O, in-situ reactivation at 423 K)					
0.0	7.8×10^{-6}	47.4	12.8	22.0	4.0
0.01	9.6×10^{-6}	66.0	14.7	9.5	1.0
0.014	11.6×10^{-6}	59.4	12.8	11.3	3.6
In-situ reactivation in H_2 pressure (other conditions: 9.6 vol% H_2O, 0.01 mol_{KOH}/mol_{Ni})					
No reactivation	7.0×10^{-6}	41.4	30.6	10.3	22.6
Reactivation at 393 K	11.7×10^{-6}	49.5	14.3	11.9	20.4
Reactivation at 423 K	9.6×10^{-6}	66.0	14.7	9.5	1.0
Reactivation at 438 K	9.4×10^{-6}	64.5	7.1	9.9	10
Water addition in vol% (other conditions: 0.01 mol_{KOH}/mol_{Ni}, in-situ reactivation at 423 K)					
0%	5.2×10^{-6}	49.3	17.0	11.9	28.6
8%	7.5×10^{-6}	59.1	13.0	14.3	4.0
9.6%	9.6×10^{-6}	66.0	14.7	9.5	1.0
10.0%	7.3×10^{-6}	64.1	15.5	12.6	6.0
12.8%	8.1×10^{-6}	56.5	11.5	11.8	10.2

Notes. Conditions: $(ADN)_0 = 0.222$ mol, $(HMDA)_0 = 0.207$ mol, H_2 pressure = 2.5 MPa, $T_R = 353$ K.

Another very important point is the possible modification of the catalyst structure in the course of reactivation and reaction steps. As mentioned above, after reduction, the Ni-containing materials exhibit Ni metal and a Mg(Al)O periclase-type phase with various extents of Ni substitution for Mg depending on the sample composition. It has been shown that the LDH structure can be reconstructed by rehydroxylation of the mixed oxide phase in an aqueous solution, using the so-called memory effect (26). This process is more difficult for the Ni-containing mixed oxides than the Mg-containing oxides (26–28). Elements about the occurrence of this phenomenon is of utmost importance since textural and acid–base properties are modified, with the appearance of strong Brønsted basic sites (29). The extent of reconstruction depends on the medium and the temperature. Moreover it is clear that in the case of the present catalysts, which have been previously reduced, the Ni^0 phase will be hardly reconstructed. This aspect has not been previously described, and its impact on ADN hydrogenation has been investigated for the AR5 catalyst. The catalytic properties of AR5 are reported without any reactivation step (direct hydrogenation at 353 K) and after in situ reactivation at various temperatures and 3.5 MPa H_2 pressure (Table 3). The selectivity to ACN is better with in situ reactivated material, and XRD patterns provide evidence of LDH structure reconstruction to some extent, very likely of the $[Mg_{1-x}Al_x(OH)_2]^{x+}(OH^-)$ type. It is worth noting that the LDH is reconstructed during the reactivation step. An in situ reactivation at 393 K does not significantly modify the XRD pattern (the presence of the LDH peak at $2\theta = 11.5^\circ$ with similar amplitude). However, the selectivity to ACN is higher after activation at 423 K. Attempts to reactivate the material at temperatures higher than 423 K lead to catalysts of slightly lower selectivity to ACN.

One could expect that the extent of reconstruction to the LDH structure will depend on the hydration degree of the medium. The latter was thus varied and data from Table 3 show that an optimum water content of ca. 9.6 vol% exists for which the selectivity to ACN is the highest. However, XRD patterns did not provide a clear distinction in the extent of the LDH reconstruction, with the exception of the experiment carried out in the water-free medium where no reconstruction occurred. Moreover, this optimum value of water content is very close to that found with Raney Ni as catalyst (10), in which case any reconstruction cannot obviously be invoked. On that account, one can anticipate that the promotion of ACN selectivity by H_2O is coming from both (i) the reconstruction of LDH with an increase in surface basicity and (ii) the formation of an hydrophilic interface at the metal surface, which makes the desorption of ACN easier, to the benefit of ADN adsorption.

The parametric study thus evidenced the most promising operating conditions to reach high ACN yield: 0.01 mol_{KOH}/mol_{Ni}, 9.6 vol% H_2O, and in situ reactivation in H_2 (3.5 MPa) of the catalyst at 423 K. Under these conditions, the influence of the material composition on the catalytic properties was approached.

Influence of catalyst composition. Table 4 presents the catalytic properties of the various samples for the hydrogenation of ADN under the standard conditions defined above. The initial rate on Raney Ni is twentyfold faster

TABLE 4

Catalytic Properties of Ni/Mg/Al/O LDH-Originated Catalysts for the Hydrogenation of Adiponitrile

Sample	ADN conversion	Initial rate (mol g^{-1} s^{-1})	TOF (h^{-1})	Selectivities (mol%) ACN	HMDA	ACH	BHT
AR39	70	5.6×10^{-6}	53	54.0	—	20.6	23
AR44	70	12.1×10^{-6}	70	54.1	6.3	17.4	14.8
AR5	70	9.6×10^{-6}	42	66.0	14.7	9.5	1.0
AR7	70	6.4×10^{-6}	41	64.6	7.5	11.1	9.2
AR6	70	3.0×10^{-6}	20	57.0	14.0	8.4	16.6
Raney Ni	70	210×10^{-6}	—	46.8	32.5	11.0	0.6

Notes. Conditions: $(ADN)_0 = 0.222$ mol, $(HMDA)_0 = 0.207$ mol, H_2 pressure = 2.5 MPa, 9.6 vol% H_2O, 0.01 mol_{KOH}/mol_{Ni}, $T_R = 353$ K, in-situ reactivation at 423 K.

than that on AR5. However, the rate slows down rapidly on Raney Ni, and 80% conversion was reached after 54 min on Raney Ni but 100 min on AR5. This might reflect different kinetic dependences or poisoning for these two materials. The experimental set-up did not allow us to carry out successive batch reactions in order to evaluate the extent of catalyst deactivation with accuracy. Sampling of the reaction medium was carried out between 50 and 90% conversion, where the ACN yield goes through a maximum value. For the sake of comparison, the catalytic properties were reported at 70% conversion.

It first appears that the initial rate ($t = 0$), expressed on a per gram basis, decreases when the Mg content increases. However, when expressed as TOF, the number of ADN molecules hydrogenated per accessible Ni site, the intrinsic activity only changes by a factor of 3 to 4 as a function of catalyst composition. The rate of ADN hydrogenation probably depends on the respective coverage of H_2 and ADN. Calorimetric studies of H_2 and acetonitrile adsorption on similar materials have shown that the heat of adsorption of both compounds is only slightly affected by the introduction of Mg (13). One may thus postulate that the moderate change of TOF in ADN hydrogenation is reflective of small changes in H_2 and ADN coverages.

Regarding the effect of catalyst composition on product selectivity, when the Mg content increases the tendency is for the HMDA selectivity to increase and the ACH selectivity to decrease, whereas the BHT selectivity goes through a minimum value. On that account, the selectivity (Table 4) and the yield (Fig. 3) to ACN are the highest for the AR5 sample.

The reaction scheme shown in Fig. 2 is composed of consecutive and parallel reactions. The selectivity to the target compounds is thus determined by (i) the consecutive hydrogenations ADN → ACN → HMDA and (ii) the consecutive and parallel transimination to ACH and BHT. The former hydrogenations obey Langmuir–Hinshelwood kinetics with competition of adsorption between hydrogen, ADN, and ACN (30). In this model, the ratio of adsorption constant $\lambda_{ACN}/\lambda_{ADN}$ is important and likely dominated by the electronic state of Ni d-band. It was found equal to 2.4 in the three-phase hydrogenation of ADN on Raney Ni (31).

On the other hand, the transimination reactions leading to ACH and BHT can occur on both Ni surface and acidic sites of the support (vide supra). On similar materials, the adsorption of ethylamine followed by calorimetry provided evidence of a decrease by 40 kJ mol^{-1} of the heat of adorption upon introduction of Mg (Mg/(Mg + Ni) = 0.23) (13). This is reflective of a surface of lower acid strength, less prone for catalyzing intra- and intermolecular transimination reactions.

To correlate any change of the acid–base properties of the materials, as well as the electronic state of Ni, the TPD of NH_3, and the IR spectroscopy of adsorbed CO were carried out.

Figure 4 shows the IR spectra of adsorbed CO in the region 2200–1750 cm^{-1}, characteristic of mono- and multicarbonyl species. It should be mentioned that bands of carbonates appeared in the spectral region 1700–1200 cm^{-1}; these carbonate species were formed by interaction of CO with basic sites (32). The high frequency broadband (A band) between 2100 and 2000 cm^{-1} can be assigned to monocarbonyl species on metal sites. On supported Ni catalysts, two bands of linearly adsorbed CO were observed at ca. 2040 and 2070 cm^{-1} (33). The former was due to CO adsorbed on unperturbated Ni^0 of facets. The latter was assigned to CO bonded on Ni^0 atoms in close interaction with an oxide phase (unreduced Ni or other oxide phase), or CO on low coordination sites. It should be mentioned that the presence of Ni^{2+} could give rise to a band at ca. 2195 cm^{-1} (33), which was never observed in our experiments.

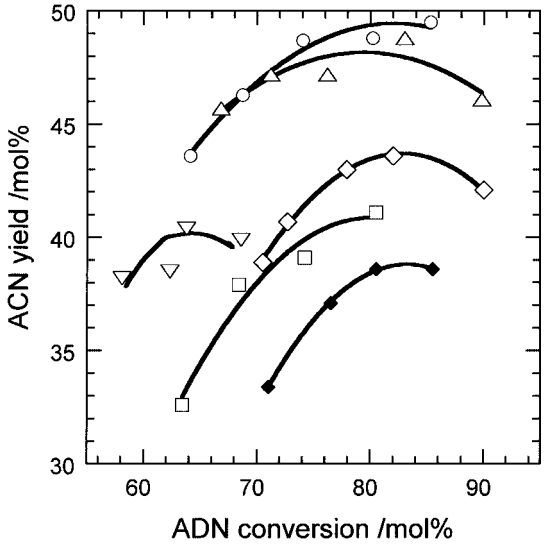

FIG. 3. Aminocapronitrile yield as a function of adiponitrile conversion in the hydrogenation of adiponitrile on AR39 (◇), AR44 (□), AR5 (○), AR6 (△), and Raney Ni (◆) catalysts; standard reaction conditions.

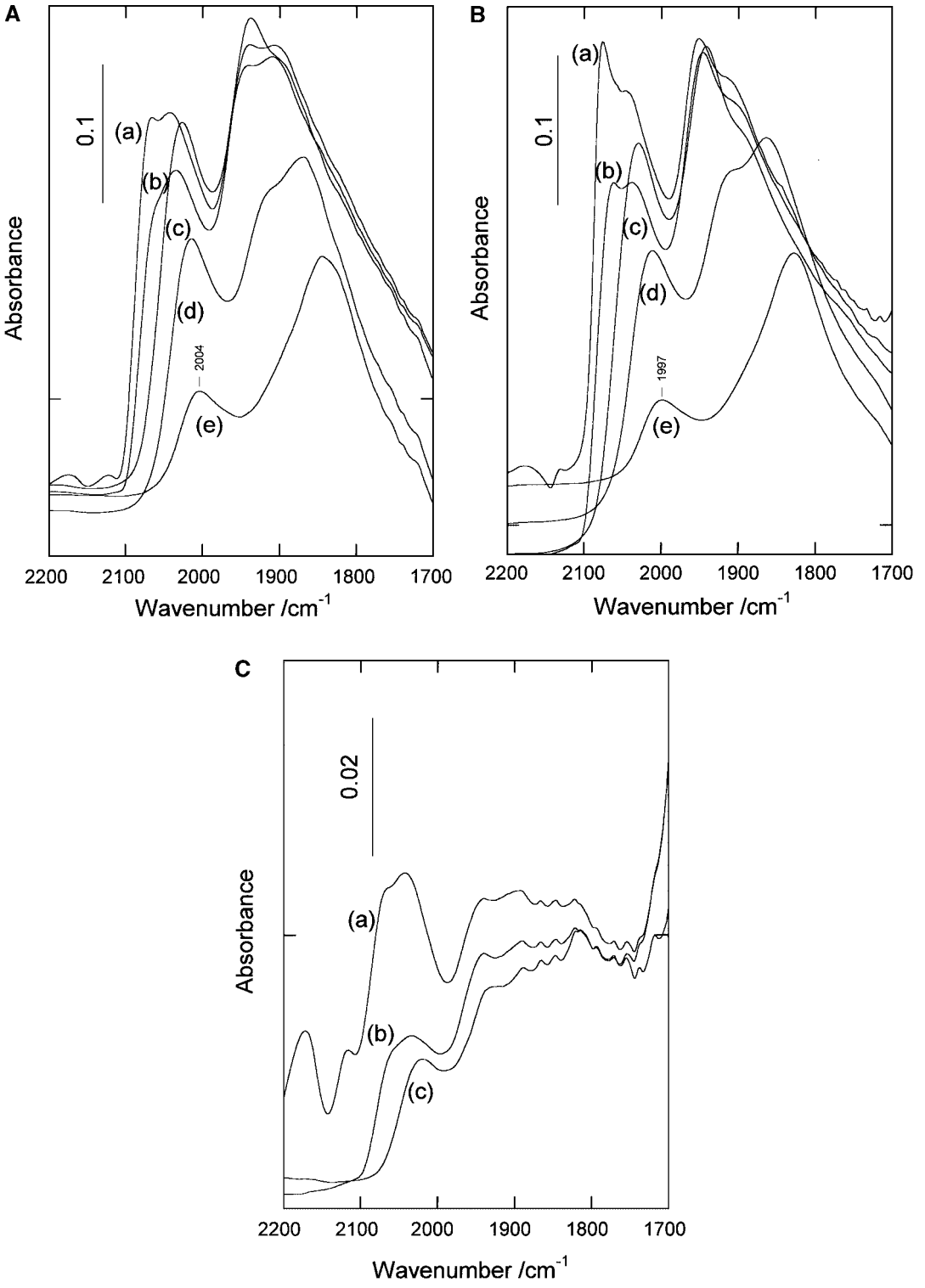

FIG. 4. (A) DRIFT spectra of adsorbed CO on in situ reduced AR39 catalysts: (a) after CO admission at 298 K, and after desorption in Ar at 298 K (b), 373 K (c), 443 K (d), 523 K (e). (B) DRIFT spectra of adsorbed CO on in situ reduced AR5 catalysts: (a) after CO admission at 298 K, and after desorption in Ar at 298 K (b), 373 K (c), 443 K (d), 523 K (e). (C) DRIFT spectra of adsorbed CO on in situ reduced AR6 catalysts: (a) after CO admission at 298 K, and after desorption in Ar at 298 K (b), 373 K (c).

The low frequency bands between 2000 and 1800 cm^{-1} (B bands) are generally assigned to multibonded CO species commonly found on Ni-based catalysts (33, 34), with ν_{CO} at ca. 1935 cm^{-1} for Ni_2CO bridged species, and below 1900 cm^{-1} for Ni_xCO multicentered species ($x = 3, 4$), at full CO coverage. The evolution of CO IR spectra at increasing desorption temperatures call forth several comments:

(1) The intensity of the A band is the highest for the AR5 sample, and more specifically that corresponding to CO on low coordination sites.

(2) The integrated intensity of the CO bands is the lowest for AR6. The decrease can be roughly estimated of one order of magnitude. However, the much lower amount of adsorbed CO might be thus accounted for by a dilution of the Ni surface by some migrating oxide species, in agreement with the lowest intensity of the B band in this sample.

(3) CO is more weakly bonded in AR6, as compared to AR39 and AR5. This is evidenced by the decrease by 80% of the integrated intensity of the A band after desorption at 373 K; band A disappeared after desorption at 413 K. A similar decrease of the A band is observed for a desorption temperature of ca. 523 K for AR39 and AR5.

(4) At low CO coverage, the ν_{CO} goes through a minimum value of 2000 cm^{-1} for AR5, as compared to 2005 cm^{-1} for AR39 and 2020 cm^{-1} for AR6. This is reflective of a larger electron back donation from Ni d-band toward the $2\pi^*$ antibonding orbital of CO. This enhanced back donation results from a higher electron density at the Ni sites.

As a concluding comment to these observations, it is shown that AR5 sample focuses attention by (i) a higher proportion of linear Ni–CO species, in particular on low coordination sites, and (ii) a stronger back donation of electrons to the antibonding CO bond. In a previous study on the gas-phase hydrogenation of acetonitrile on a catalyst from Co/Ni/Mg/Al LDH, we proposed that the transimination reactions at the Ni sites occur through a Langmuir–Hinshelwood mechanism between two vicinal multibonded adsorbed species (35). The introduction of Co dilutes the Ni phase in small ensembles less prone to accommodate neighboring multibonded species. One can propose that the presence of monocarbonyl Ni–CO species in higher proportion in AR5 reflects the presence of smaller Ni ensembles. Moreover, an increase of the electron density at Ni sites might decrease the adsorption strength of the "more basic" compound ACN with comparison to ADN. From these deductions one can understand that among the various samples, AR5 would be the less prone to favor the formation of byproducts through transimination at the metal sites.

However, as mentioned above the transimination reaction can also take place through bifunctional catalysis involving metal and acid sites. The latter sites are responsible for the rate determining step of condensation between amine and protonated imine.

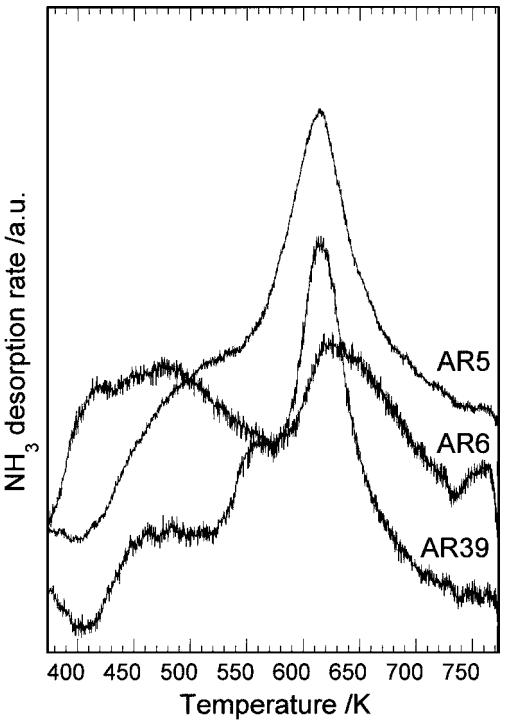

FIG. 5. NH_3-TPD profiles of AR39, AR5, and AR6; ramp: 10 K min^{-1}.

Figure 5 shows the NH_3-TPD plots of some samples. The amounts of NH_3 desorbing during these experiments are of 0.35, 0.77, 0.85, and 0.60 $mmol_{NH3}$ g^{-1} for samples AR39, AR44, AR5, and AR6, respectively. It is shown that the amount of NH_3 adsorbed increases with the Mg content, but concurrently the proportion of NH_3 strongly bonded decreases with the appearance of a broad desorption peak between 373 and 673 K. One can postulate the appearance of weaker acid sites upon Mg substitution for Ni, probably associated to Mg^{2+} belonging to acid–base pairs (22). Weaker acid sites upon Mg introduction have been indeed identified previously by calorimetry of ethylamine adsorption on similar materials (13). The antagonistic evolution of number and strength of acid sites as a function of the Mg content in the material makes them difficult to propose a correlation between acidity and condensed products formed through transimination reactions on the acid sites.

CONCLUSIONS

Ni/Mg/Al LDHs constitute good candidates as precursors of catalysts for the hydrogenation of ADN into ACN with good yields. The catalyst obtained from Ni/Mg/Al (0.60/0.15/0.25, AR5), calcined at 393 K and reduced at 823 K, exhibits the highest selectivity and yield to ACN (66% selectivity at 70% conversion, 50% yield at 85% conversion). We suggest that this behavior comes from (i) a faster desorption of ACN thus decreasing the consecutive hydrogenation to HMDA and (ii) the lowering of the

undesired consecutive transimination reactions which can occur on both the acid and the metal sites between imines- and amines-like adsorbed species. The transimination on the metal sites could occur through a Langmuir–Hinshelwood mechanism between multibonded adsorbed species. This reaction is not favored on small Ni^0 ensembles, which are found on the AR5 sample. It was impossible to conclude on a positive effect of Mg substitution for Ni with respect to the bifunctional-catalyzed transimination since upon introduction of Mg the number of acid sites increases but their strength decreases. Finally, the ACN desorption would be the fastest on the AR5 sample thanks to a higher electron density at the Ni sites, as evidenced by IR spectroscopy of adsorbed CO.

ACKNOWLEDGMENT

A.R. thanks the Rhodia company for a scholarship.

REFERENCES

1. McCoy, M., *Chem. Eng. News* **78**(40), 32 (2000).
2. German Patent 848 654 (1952) to BASF.
3. Medina, F., Salagre, P., Sueiras, J. E., and Fierro, J. L. G., *Appl. Catal., A* **92**, 131 (1992).
4. Medina, F., Salagre, P., Sueiras, J. E., and Fierro, J. L. G., *J. Chem. Soc. Faraday Trans.* **89**, 3981 (1993).
5. Mares, F., Galle, J. E., Diamond, S. E., and Regina, F. J., *J. Catal.* **112**, 145 (1988).
6. U.S. Patent 4,389,348 (1983) to Allied Signal Corporation.
7. Patent WO9947492 (1999) to Dupont de Nemours.
8. Patent WO9944984 (1999) to BASF.
9. Ziemecki, S. B., *in* "Heterogeneous Catalysis and Fine Chemical III" (M. Guisnet, J. Barbier, J. Barrault, C. Bouchoule, D. Duprez, G. Pérot, and C. Montassier, Eds.), p. 283. Elsevier, Amsterdam, 1993.
10. Patent WO9618603 (1995) to Rhône Poulenc.
11. Marion, Ph., Grenouillet, P., Jenck, J., Joucla, M., *in* "Heterogeneous Catalysis and Fine Chemical II" (M. Guisnet, J. Barrault, C. Bouchoule, D. Duprez, G. Pérot, R. Maurel, and C. Montassier, Eds.), p. 329. Elsevier, Amsterdam, 1991.
12. de Bellefon, C., and Fouilloux, P., *Catal. Rev.-Sci. Eng.* **36**, 459 (1994).
13. Medina Cabello, F., Tichit, D., Coq, B., Vaccari, A., and Dung, N. T., *J. Catal.* **167**, 142 (1997).
14. Tichit, D., Medina Cabello, F., Durand, R., Mateo, C., Coq, B., Sueiras, J. E., and Salagre, P., *in* "Heterogeneous Catalysis and Fine Chemical IV" (H. U. Blaser, A. Baiker, and R. Prins, Eds.), p. 297. Elsevier, Amsterdam, 1997.
15. von Braun, J., Blessing, G., and Zobel, F., *Chem. Ber.* **36**, 1988 (1923).
16. Dallons, J. L., Van Gysel, A., and Jannes, G., *in* "Catalysis of Organic Reactions" (W. E. Pascoe, Ed.), p. 93. Dekker, New York, 1992.
17. Pavlenko, N. V., Tripol'skii, A. I., Prokhorenko, E. V., and Golodets, G. I., *Kinet. Katal.* **28**, 1382 (1987).
18. Hochard, F., Jobic, H., Massardier, J., and Renouprez, A. J., *J. Mol. Catal.* **95**, 165 (1995).
19. Freidlin, L. Kh., Sladkova, T. A., and Englina, F. F., *Kinet. Katal.* **3**, 417 (1962).
20. Verhaak, M. J. F. M., Van Dillen, A. J., and Geus, J. W., *Catal. Lett.* **26**, 37 (1994).
21. Patent WO9710052 (1996) to Rhône Poulenc.
22. Prinetto, F., Ghiotti, G., Durand, R., and Tichit, D., *J. Phys. Chem. B* **104**, 11,117 (2000).
23. Tichit, D., Medina, F., Coq, B., and Dutartre, R., *Appl. Catal., A* **159**, 241 (1997).
24. Turlier, P., Praliaud, H., Moral, P., Martin, G. A., and Dalmon, J. A., *Appl. Catal.* **19**, 287 (1986).
25. Thomas-Pryor, S. N., Manz, T. A., Liu, Z., Koch, T. A., Sangupta, S. A., and Delgass, W. N., *in* "Catalysis of Organic Reactions" (F. Herkes, Ed.), p. 195. Dekker, New York, 1998.
26. Sato, K., Wakabayasi, T., and Shimada, M., *Ind. Eng. Chem. Prod. Res. Dev.* **25**, 89 (1986).
27. Sato, K., Fujita, H., Endo, T., Shimada, M., and Tnunashima, A., *React. Solids* **5**, 219 (1988).
28. Rebours, B., d'Espinose de la Caillerie, J. B., and Clause, O., *J. Am. Chem. Soc.* **116**, 1707 (1994).
29. Prinetto, F., Tichit, D., Teissier, R., and Coq, B., *Catal. Today* **55**, 103 (2000).
30. Mathieu, C., Dietrich, E., Delmas, H., and Jenck, J., *Chem. Eng. Sci.* **47**, 2289 (1992).
31. Joly-Vuillemin, C., Gavroy, D., Cordier, G., de Bellefon, C., and Delmas, H., *Chem. Eng. Sci.* **49**, 4839 (1994).
32. Lavalley, J. C., *Catal. Today* **27**, 377 (1996).
33. Primet, M., Dalmon, J. A., and Martin, G. A., *J. Catal.* **46**, 25 (1977).
34. Eischens, R. P., and Pliskin, W. A., *in* "Advances in Catalysis" (D. D. Eley, W. G. Frankenburg, V. I. Komarevski, and P. B. Weisz, Eds.), Vol. 10, p. 1. Academic Press, San Diego, 1958.
35. Coq, B., Tichit, D., and Ribet, S., *J. Catal.* **189**, 117 (2000).